Cement and Concrete Research 151 (2022) 106620

Contents lists available at ScienceDirect

Cement and Concrete Research

journal homepage: www.elsevier.com/locate/cemconres

Solubility and speciation of iron in cementitious systems

Fabio E. Furcas [a,*], Barbara Lothenbach [b], O. Burkan Isgor [c], Shishir Mundra [a], Zhidong Zhang [a], Ueli M. Angst [a]

[a] Institute for Building Materials, ETH Zürich, Stefano-Franscini-Platz 3, 8093 Zürich, Switzerland
[b] Empa, Concrete & Asphalt Laboratory, Switzerland
[c] School of Civil and Construction Engineering, Oregon State University, Corvallis, OR, USA

ARTICLE INFO

Keywords:
Pore solution
Corrosion
Reaction
Chloride
pH
Durability
Modelling

ABSTRACT

Aqueous iron hydrolysis products and chloride complexes influence steel corrosion kinetics and dictate the amount and type of corrosion products formed. Here, we compile a thermodynamic database devoted to aqueous iron species and solid oxides as well as chloride complexes, aiming to describe their speciation and solubility within the prevailing chemical environment of interest for cementitious systems. We compare thermodynamic calculations to empirical data on the elemental composition of pore solutions from cementitious systems.

It is found that dissolved iron concentrations in cement pore solutions can differ considerably from thermodynamic predictions. In particular, measured Fe(II) concentrations can exceed the thermodynamic limit by 2–5 orders of magnitude. Additionally, experimentally obtained iron solubility in the presence of chloride exceed thermodynamic predictions. We discuss that these differences may be explained by so far unknown iron complexes, stabilisation of intermediate phases such as chloride green rust, or due to (kinetic) hindrance of precipitation.

1. Introduction

Steel corrosion is the most common cause of premature deterioration of reinforced concrete structures. Given the substantial economic impact associated with this durability problem [1,2], numerical modelling of reinforcement corrosion has received increasing levels of attention in recent years [3–8]. However, predicting the durability of reinforced concrete structures exposed to corrosive conditions remains to be a considerable challenge [9].

Chlorides, if present at sufficiently high quantities at the steel-concrete interface, can lead to the breakdown of the passive film that typically forms on steel surfaces in the alkaline environment of concrete [10–12]. Another possible cause for steel corrosion in concrete is carbonation of the cementitious phases and the associated loss in pH buffering capacity of the matrix surrounding the steel [13,14]. Motivated by these causes for corrosion, the modelling of chloride ingress and concrete carbonation in concrete has been a subject of research for a long time as evidenced by a range of ever-evolving (reactive) transport models for quantifying the space-time evolution of species that initiate corrosion of reinforcement [15–18]. However, comparatively little research has been devoted to fundamentally understanding and modelling the transport and reaction processes of the iron species that are released into the cementitious matrix after corrosion initiation. Being able to reliably predict the transport processes and reactions of these iron species, however, is important for several reasons. First, it is well known that the corrosion kinetics of a metal is strongly influenced by mass transport in the electrolyte around the metal surface [19–22]. Second, the transport and precipitation of iron species in the cementitious matrix surrounding the steel are important steps that need to be considered in predicting corrosion-related damage of concrete structures, such as cracking and spalling [3–5,7,8,18,23–26].

Corrosion-induced damage in concrete is associated with the expansive pressure that can be generated from the formation of corrosion products as a result of the conversion of dissolved iron ions into various solid products. When allowed to precipitate, these products have specific volumes up to ~2–6 times larger than that of Fe(0). Accurate prediction of damage caused by steel corrosion in concrete requires the knowledge of the type and amount of corrosion products as well as the location where they form in concrete. While it is now well established that corrosion products can form away from the reinforcement and their distribution in concrete typically has a non-uniform pattern [27–29], most existing corrosion-induced damage models assume partial or full

* Corresponding author.
E-mail address: ffurcas@ethz.ch (F.E. Furcas).

https://doi.org/10.1016/j.cemconres.2021.106620
Received 14 May 2021; Received in revised form 3 September 2021; Accepted 25 September 2021
Available online 6 October 2021

corrosion product formation around the circumference of steel reinforcement, which is an oversimplification of the problem [23–26].

In the sequence of events initiated by chloride ingress, namely accelerated electro-dissolution of steel followed by ferrous ion transport and reactions that may lead to corrosion product precipitation, comparatively little research has been conducted on the role of chlorides beyond their function as a catalyst in electrochemical iron dissolution [27,30]. As a consequence, the question as to whether the presence of chlorides solely facilitates the electro-dissolution of iron or whether it furthermore influences corrosion product precipitation and transport remains unanswered to date. A number of publications, both based on practical experience and dedicated laboratory or modelling studies, support the hypothesis that iron transport is facilitated by the formation of an intermediary chloro-complex, controlling the solubility of iron at high pH [25,27,30,31]. However, limited data is available that allows for a quantitative description of the different iron species reactions involved and how their thermodynamics and kinetics play a role in the mechanism of chloride-induced corrosion and subsequent concrete damage.

The objective of this work is to investigate the solubility and competitive formation of corrosion products and their sensitivity to changes in the concentration of precipitation-inhibiting solutes. To enable a comparison between experimentally measured and thermodynamically predicted aqueous iron concentrations, empirical data are first reviewed on the elemental composition of pore solutions pressed from hardened concrete or in equilibrium with cementitious phases. Subsequently, a thermodynamic database is presented to comprise state-of-the-art data for all aqueous iron species and solid oxides relevant for the formation of corrosion products. Where applicable, experimental data are presented for benchmarking thermodynamic parameters accepted to the database. With regard to the discussion on chloro-complexation limiting the solubility of iron at high pH, particular emphasis is put on the thermodynamics of chloride green rust. To account for the effect of iron up-take into and release by hydrated clinker other iron bearing phases, their mineralogy as well as the influence of supplementary cementitious materials (SCM) is furthermore discussed. The comparison of thermodynamic simulation results allows a critical assessment of the applicability of thermodynamic modelling to simulate iron dissolution and speciation in cementitious systems.

2. Review of empirical data on iron phases in cementitious systems

Empirical data on total iron concentration in cementitious systems is available generally from studies investigating the pore solution composition of cement paste, mortar or concrete produced from different cements [32–41]. The total concentration of iron in the pore solution of cementitious systems varies significantly depending on the types and relative amounts of cementitious materials (Portland cement (PC) and SCM, in particular, blast furnace slag), the degree of hydration of the system, and the pH of the pore solution [33–35]. These measurements can also be affected by the experimental methods used to quantify iron, and some of the parameters of the tests such as the equilibration time [33–40]. In general, existing literature on iron phases in concrete pore solutions may be subdivided into two categories (i) those investigating pore solutions pressed from solid concrete, mortar, or paste; and (ii) those studying aqueous solutions that were equilibrated with synthesised iron-containing hydrates in a controlled laboratory environment. The mineralogical constituents of both types of systems are capable of releasing iron into the pore solution and taking up iron from the pore solution. However, the most predominant iron-bearing phase in PC may shift, depending on the equilibration time and pH [42]. As the introduction of blast-furnace slag and other SCMs at common substitution levels may furthermore alter pH and phase assemblage [43], it is important to discriminate between systems synthesised naturally and in a controlled laboratory environment. For this purpose, the main iron bearing phases in PC are reviewed alongside the solubility-limiting iron oxide corrosion products in Section 3.

Fig. 1 illustrates the ranges of selected aqueous iron concentrations as reported from experimental studies. The data are grouped according to the iron oxidation state, the type of cementitious system, and the presence or absence of silica. To exclude potential effects of equilibration time, only measurements for equilibration times larger than 1 day were considered. As shown in Fig. 1, reported measurements vary significantly in the literature. Reported Fe(III) concentrations range between 2 and 5×10^{-6} M in the pore solution of systems produced from PC with and without partial fly ash replacement [34]. In systems produced from PC with partial silica fume replacement, low Fe(III) concentrations close to 10^{-7} M were observed [33]. Somewhat higher iron concentrations of up to $\sim 10^{-4}$ M were reported in the pore solution of a cementitious system containing blast furnace slag (CEM III/B cement) [35]. Blast furnace slags commonly contain micro-sized Fe(0), which can react slowly affecting the redox state of iron in the pore solution [44,45] and thus affect iron concentrations. Andersson et al. [41] consistently measured a total iron concentration of $\sim 10^{-5}$ M across a variety of cementitious systems, including PC, high alumina cement, and blast furnace slag cement.

Aqueous iron concentrations in equilibrium with synthesised cementitious phases range from 1.2×10^{-5} to 3.0×10^{-7} M, depending on pH, and the presence of silica and/or carbonates. In these experiments, the precipitation of $Fe(OH)_3$(s) is commonly observed in addition to Fe(III)-containing hydrate phases, such as hydrogarnet[1] [36] and carbonate containing AFm phases [37,38]. This observation underlines that the sparingly soluble $Fe(OH)_3$(s) marks the upper solubility limit for Fe(III) in cementitious systems [46,47].

At high pH values, Fe(II) concentrations up to 10^{-3} M were observed [32]. Mancini et al. [32] remarked the particular challenges associated to investigations of Fe(II) interactions with calcium-silicate-hydrate (C-S-H) phases due to the limited stability of Fe(II) at alkaline conditions. As far as we know, Ref. [32] is the only attempt made to investigate Fe (II) interactions with cementitious phases to date. Irrespective of the chemical environment and iron oxidation state, the upper solubility bounds are dictated by the respective solubility controlling iron (hydr) oxides. The Fe(II) concentrations shown in Fig. 1 appear to be much higher than those predicted by the dissolution of $Fe(OH)_2$(s), which are of the order of 10^{-7}–10^{-6} M. Possible reasons for this discrepancy will be discussed later in this paper.

A particular influencing factor on iron solubility is seen to be the presence of chlorides. In this regard, it has been hypothesized that the solubility of iron in sufficiently chloride rich solutions is controlled by chloro-complexation. Sagoe-Crentsil and Glasser [30] investigated the solubility of iron in artificial alkaline concrete pore solution electrolytes of similar composition under varying chloride concentrations. Powder X-ray spectroscopy measurements confirmed the formation of a mixed Fe(II)-Fe(III) chloro-solid ($(Fe^{2+})_3(Fe^{3+})(OH)_8Cl{\cdot}nH_2O$), commonly referred to as chloride green rust ($GR(Cl^-)$), at high pH, together with trace amounts of δ-FeOOH(s) for chloride concentrations >30 mM. Likewise, the total soluble iron concentration appears to sharply increase to values of ≈170–180 mM for $[Cl^-] > 15$ mM. Further analysis of a $[Cl^-] = 30$ mM solution showed an Fe(II)/Fe(III) ratio of approximately 3.5, similar to that of $GR(Cl^-)$.

Understanding the formation of the sparingly soluble iron solids, ascertaining their regimes of stability and sensitivity to changes in the concentration of co-reacting species is paramount to gain insights into the behaviour of iron in cementitious pore solutions. To enable a comparison between empirical and thermodynamically predicted Fe(II) and Fe(III) concentrations and explore the possibility of chloro-complexation dictating the solubility limit, thermodynamic modelling is used as described in the following section.

[1] $Ca_3(Al_xFe_{1-x})_2(SiO_4)_y(OH)_4$.

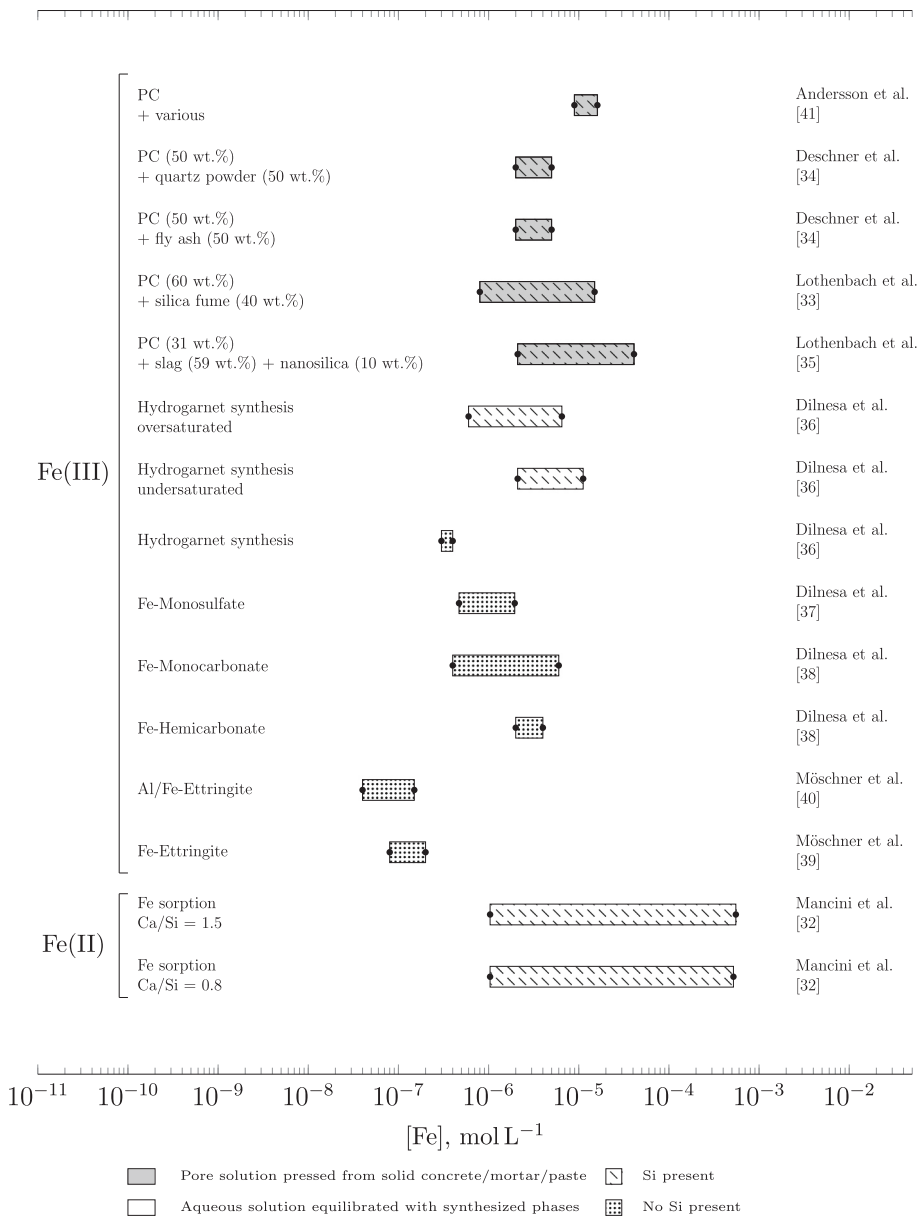

Fig. 1. Compilation of literature data on aqueous iron concentrations, measured with different experimental approaches (see text for explanations). The data is grouped according to the iron oxidation state, type of cementitious system and the presence or absence of silica. For all studies reviewed, measurements taken for equilibration times less than 1 day are omitted. All presented values correspond to the iron concentration at T ~ 20 °C.

3. Thermodynamic data for iron and modelling

3.1. Method of data selection

The solubility and complex formation of iron species has been studied extensively over the last century. In total, more than 15 solid iron (hydr)oxides (i.e., iron oxides, oxyhydroxides, and hydroxides) and more than 40 aqueous phase reactions are characterised to date [46,48] Under the premise of a complete thermodynamic database including all relevant complexes and solids, thermodynamic modelling can reliably predict the equilibrium composition at given pressure (P), volume (V) and temperature (T). The thermodynamic database presented in this section aims to fulfil this demand.

In the process of data selection, particular emphasis is put on aqueous iron species and solid oxides important to the formation of corrosion products and corrosion initiation in concrete. Components selected are either (i) reported to be thermodynamically stable at the system conditions of interest, or (ii) have been reported to exist in competition with the predominant phases formed, or (iii) are a thermodynamically unstable kinetic precursor to them. For a detailed review of the selection procedure adopted to compute thermodynamic parameters gathered from multiple experimental sources, the reader is referred to Lemire et al. [46,48] and Brown and Ekberg [49]. Likewise, the chemical thermodynamics of iron-bearing cementitious phases is extensively reviewed in a previous work [50]. In this paper, the importance on the solubility of iron in cementitious systems is elucidated further in Section 4.4.

3.2. Thermodynamic database

Table 1 lists various molar Gibbs free energies ($\Delta_f G_m^\circ$, $\Delta_r G_m^\circ$) and enthalpies ($\Delta_f H_m^\circ$, $\Delta_r H_m^\circ$) of formation and reaction (indices f and r, respectively), and entropies (S_m°, $\Delta_r S_m^\circ$), along with the corresponding specific heats and molar volumes of selected iron-containing species.

Table 1
: Summary of dependent reaction components as defined by the corrosion related hydrolysis and dissolution reactions enlisted in Table 2.

Component	MW, g mol^{-1}	$\Delta_f G_m^\circ$, kJ mol^{-1}	$\Delta_f H_m^\circ$, kJ mol^{-1}	S_m°, J mol^{-1} K^{-1}	$C_{p,m}^\circ$, J mol^{-1} K^{-1}	V°, J bar^{-1}	Source
α-Fe(0)	55.8450	0	0	27.1 ± 0.2	25.1 ± 0.5	0.71	[46]: S_m°, $C_{p,m}^\circ$, [53]: V°
Fe^{2+}	55.8450	−90.72 ± 0.64	−90.3 ± 0.5	−102.2 ± 2.8	−23.0 ± 10.0	−2.26[a]	[46]
Fe^{3+}	55.8450	−16.23 ± 0.65	−50.1 ± 1.0	−282.4 ± 3.9	−108.0 ± 20.0	−3.78[a]	[46]
Fe(II) hydrolysis products							
$FeOH^+$	72.8523	−274.00 ± 0.86[b]	−321.5 ± 0.1	−29.6 ± 4.9	63.1[a]	−1.67[a]	[49]
$Fe(OH)_2$(aq)	89.8597	−447.80 ± 0.79[b]	−546.6 ± 1.1	31.9 ± 4.9			[49]
Fe(O)(aq) (+H_2O(l) = $Fe(OH)_2$(aq))	71.8444	−210.69 ± 0.79[c]	−260.7 ± 1.1[c]	−38.0 ± 4.9	−0.0[a]	−1.65[a]	
$Fe(OH)_3^-$	106.867	−615.49 ± 1.08[c]	−807.5 ± 2.3	−47.4 ± 8.6			[49]
FeO_2H^- (+H_2O(l) = $Fe(OH)_3^-$)	88.8518	−378.39 ± 1.08[c]	−521.7 ± 2.3[c]	−117.4 ± 8.6	92.8[a]	−1.35[a]	
Fe(III) hydrolysis products							
$FeOH^{2+}$	72.8523	−240.77 ± 0.66[b]	−292.6 ± 1.1	−109.3 ± 5.5	−33.7[a]	−2.53[a]	[49]
$Fe(OH)_2^+$	89.8597	−457.84 ± 0.87[b]	−418.9 ± 0.7	−11.8 ± 4.9			[49]: $\log_{10}\beta^\circ$, [52]: $\Delta_r H_m^\circ$
FeO^+ (+H_2O(l) = $Fe(OH)_2^+$)	71.8444	−220.74 ± 0.87[c]	−133.1 ± 0.7[c]	−81.8 ± 4.9	−200.9[a]	−4.20[a]	
$Fe(OH)_3$(aq)	106.867	−657.56 ± 1.63[b]	−761.2 ± 4.9	182.4 ± 17.6			[49]
FeO_2H(aq) (+H_2O(l) = $Fe(OH)_3$(aq))	88.8518	−420.45 ± 1.63[c]	−475.4 ± 4.9[c]	113.5 ± 17.6	−312.1[a]	0.72[a]	
$Fe(OH)_4^-$	123.874	−841.35 ± 1.47[b]	−1046.6 ± 2.1	76.2 ± 9.1			[49]
FeO_2^- (+$2H_2O$(l) = $Fe(OH)_4^-$)	87.8438	−367.14 ± 1.47[c]	−474.9 ± 2.1[c]	6.3 ± 9.1	−234.9[a]	0.05[a]	
$Fe_2(OH)_2^{4+}$	145.705	−490.05 ± 1.36[b]	−641.7 ± 9.7	−379.7 ± 33.5			[49]
$Fe_3(OH)_4^{5+}$	235.564	−961.13	−1234.5	−490.1			[54]
Fe(II) chloride complexes							
$FeCl^+$	91.298	−216.23 ± 4.61[b]	−235.8 ± 1.8	7.6 ± 16.8	86.5[a]	0.09[a]	[46]
$FeCl_4^{2-}$	197.657	−584.74 ± 3.35[b]	−687.2 ± 2.6	260.2 ± 7.6			[55]
Fe(III) chloride complexes							
$FeCl^{2+}$	91.298	−156.12 ± 0.87	−194.7 ± 4.7	−121.3 ± 16.0	14.8[a]	−2.29[a]	[46]
$FeCl_2^+$	126.751	−291.33 ± 1.44[b]	−342.39 ± 8.7[e]	13.6 ± 33.6[e]	300.7[a]	1.03[a]	[46]: $\log_{10}\beta^\circ$, [56]: $\Delta_r H_m^\circ$
$FeCl_3$(aq)	162.204	−415.87 ± 1.68	−494.7 ± 11.3[e]	97.4 ± 50.9[e]	368.2[a]	3.59[a]	[46]: $\log_{10}\beta^\circ$, [56]: $\Delta_r H_m^\circ$
$FeCl_4^-$	197.657	−536.87 ± 3.07	−654.2 ± 11.4[e]	144.9 ± 64.3[e]			[56]
Mixed Fe(II) and Fe(III) iron chloride solids							
$(Fe^{2+})_3(Fe^{3+})(OH)_8Cl{\cdot}nH_2O$[f]	430.922	−2605.22 ± 0.97			487.0[d]	3.65	[57], [58]: V°
Solid Fe(II) iron hydr(oxides)							
FeO(s), ferrous oxide	71.8444	−251.40 ± 2.20	−272.0 ± 2.1	60.0 ± 1.7		1.20	[53]
$Fe(OH)_2$(s), white rust	89.8597	−494.89 ± 5.07[b]	−583.4[g]	84.0[g]	~90.0[g]	2.95	[49]: $\log_{10}\beta^\circ$, [59], [60]: V°
Solid Fe(III) iron hydr(oxides)							
α-Fe_2O_3(s), hematite	159.688	−744.45 ± 2.63	−826.3 ± 2.6	87.4 ± 0.2	103.9 ± 0.2	3.03	[46], [53]: V°
γ-Fe_2O_3(s), maghemite	159.688	−727.83 ± 3.03	−808.0 ± 3.0	93.0 ± 0.4	104.7 ± 0.4	3.28	[46], [61]: V°
α-FeOOH(s), goethite	88.8518	−489.54 ± 2.00	−560.5 ± 2.0	59.7 ± 0.5	74.4 ± 0.4	2.09	[46], [61]: V°
β-FeOOH(s), akaganéite	88.8518	−486.53 ± 2.77	−551.5 ± 2.2	79.9 ± 1.0	91.5 ± 0.2	2.55	[46], [62]: V°
γ-FeOOH(s), lepidocrocite	88.8518	−479.81 ± 2.60	−549.2 ± 2.0	65.1 ± 0.5	69.1 ± 0.6	2.24	[46], [61]: V°
δ-FeOOH(s), feroxyhie	88.8518	−478.10 ± 2.00[h]	−547.4 ± 1.3	65.0 ± 5.0			[63]
$Fe(OH)_3$(s), ferrihydrite, 2-line	106.867	−708.50 ± 2.00	−827.1 ± 2.0	127.6 ± 5.4[i]	~152.0 ± 5.0	3.40	[38], [64]: V°
$Fe(OH)_3$(s), ferrihydrite, 6-line	106.867	−711.00 ± 2.00	−830.3 ± 2.0	126.5 ± 4.3[i]	~152.0 ± 5.0	3.40	[38], [64]: V°
Mixed Fe(II) and Fe(III) iron hydr(oxides)							
α-Fe_3O_4(s), magnetite	231.533	−1012.72 ± 1.61	−1115.8 ± 1.6	145.9 ± 0.3	150.8 ± 1.3	4.45	[46], [53]: V°

[a] Retrieved via the HKF EOS [51].
[b] Internally computed from $\Delta_r G_m^\circ = \sum_i \nu_i \Delta_f G_{m,i}^\circ$.
[c] Obtained by subtracting $\Delta_f G_m^\circ(H_2O(l)) = -237.140 \pm 0.041$ kJ mol^{-1} and $\Delta_f H_m^\circ(H_2O(l)) = -285.830 \pm 0.040$ kJ mol^{-1} [46] from the previously enlisted species.
[d] From $\Delta_f C_{p,m}^\circ$.
[e] Value computed based on $\Delta_f H_m^\circ$ estimated from Liu et al. [56] against the explicit recommendation of Lemire et al. [46] and included here for the sake of completeness.
[f] Thermodynamic parameters and uncertainties tabulated for $n = 2$, based on $\mu^\circ(3Fe(OH)_2{\cdot}Fe(OH)_2Cl) = -509{,}325 \pm 230$ cal mol^{-1} [57].
[g] Values enlisted against the explicit recommendation of Lemire et al. [46].
[h] Value corresponding to poorly crystalline samples with specific surface areas of 88 m^2 g^{-1}.
[i] Averaged value based on the upper and lower range of S_m° as reported by Majzlan et al. [64].

Associated equilibrium solubility products and formation constants are presented in Table 2. Where available, the data selected in the recent reviews of Brown and Ekberg [49] and of Lemire et al. [46,48] are used, and these are complemented with additional data for chloride containing complexes and solids. Reactions for which $\Delta_r H_m^\circ$ is unknown presently are considered to be isoentropic. Where indicated, partial molar volumes and heat capacities of aqueous species are retrieved via the revised HKF equation of state [51]. Auxiliary data for co-reacting species are taken from the Nagra/PSI thermodynamic database [52]. The default Nagra/PSI thermodynamic database [52] was completed with aqueous and solid phase iron species based on recent reviews [46,48,49] as reported in Tables 1 and 2.

3.3. Calculation methodology

All calculations shown later in this paper were performed using the GEM-Selektor (GEMS3K) software package. GEMS is a multi-purpose thermodynamic modelling framework, capable of computing

Table 2
: Summary of the thermodynamic parameters of hydrolysis and formation reactions defining dependent components presented in Table 1.

Reaction	$\log_{10}\beta^\circ$	a	b	c	$\Delta_r H_m^\circ$, kJ mol^{-1}	Source
Fe(II) hydrolysis products						
$Fe^{2+} + H_2O(l) \rightleftharpoons FeOH^+ + H^+$	−(9.43 ± 0.10)	0.136	−2851	0	54.6 ± 0.9	[49]
$Fe^{2+} + 2H_2O(l) \rightleftharpoons Fe(OH)_2(aq) + 2H^+$	−(20.52 ± 0.08)	−0.291	−6030	0	115.4 ± 1.0	[49]
$Fe^{2+} + 2H_2O(l) \rightleftharpoons Fe(OH)_3^- + 3H^+$	−32.68 ± 0.15)	−8.10	−7330	0	140.3 ± 2.2	[49]
Fe(III) hydrolysis products						
$Fe^{3+} + H_2O(l) \rightleftharpoons FeOH^{2+} + H^+$	−(2.20 ± 0.02)	5.393	−2263	0	43.3 ± 0.6	[49]
$Fe^{3+} + 2H_2O(l) \rightleftharpoons Fe(OH)_2^+ + 2H^+$	−(5.17 ± 0.10)	–	–	–	71.5	[49]: $\log_{10}\beta^\circ$, [52]
$Fe^{3+} + 3H_2O(l) \rightleftharpoons Fe(OH)_3(aq) + 3H^+$	−(12.26 ± 0.26)	66.0	−9987	−7.86	146.3 ± 4.8	[49]
$Fe^{3+} + 4H_2O(l) \rightleftharpoons Fe(OH)_4^- + 4H^+$	−(21.60 ± 0.23)	4.12	−7669	0	146.8 ± 1.8	[49]
$2Fe^{3+} + 2H_2O(l) \rightleftharpoons Fe_2(OH)_2^{4+} + 2H^+$	−(2.91 ± 0.07)	–	–	–	30.1 ± 9.5	[49]
$3Fe^{3+} + 4H_2O(l) \rightleftharpoons Fe_3(OH)_4^{5+} + 4H^+$	−(6.30 ± 0.00)	–	–	–	59.0 ± 0.0	[54]
Fe(II) chloride complexes						
$Fe^{2+} + Cl^- \rightleftharpoons FeCl^+$	−(1.00 ± 0.80)[a]	–	–	–	21.6 ± 1.8	[46]
$Fe^{2+} + 4Cl^- \rightleftharpoons FeCl_4^{2-}$	−(5.40 ± 0.57)[b]	–	–	–	71.4 ± 2.5	[55]
Fe(III) chloride complexes						
$Fe^{3+} + Cl^- \rightleftharpoons FeCl^{2+}$	+(1.52 ± 0.10)	–	–	–	22.5 ± 4.6	[46]
$FeCl^{2+} + Cl^- \rightleftharpoons FeCl_2^+$	+(0.70 ± 0.20)	–	–	–	19.4 ± 7.3[c]	[46]: $\log_{10}\beta^\circ$, [56]: $\Delta_r H_m^\circ$
$FeCl_2^+ + Cl^- \rightleftharpoons FeCl_3(aq)$	−(1.17 ± 0.15)	–	–	–	14.8 ± 7.3[c]	[46]: $\log_{10}\beta^\circ$, [56]: $\Delta_r H_m^\circ$
$FeCl_3(aq) + Cl^- \rightleftharpoons FeCl_4^-$	−(1.79 ± 0.45)	–	–	–	7.5 ± 1.5[c]	[56]
Mixed Fe(II) and Fe(III) iron chloride solids						
$4Fe(OH)_2(s) + Cl^- + H^+ + nH_2O(l) \rightleftharpoons GR(Cl^-)(s) + ½\ H_2(g)$	−(9.36 ± 0.31)[d]	–	–	–	–	[57]
Solid Fe(II) iron hydr(oxides)						
$Fe^{2+} + 2H_2O(l) \rightleftharpoons Fe(OH)_2(s)$, White Rust $+ 2H^+$	−(12.27 ± 0.88)	–	–	–	–	[49]
Solid Fe(III) iron hydr(oxides)						
$Fe^{3+} + 3/2\ H_2O(l) \rightleftharpoons ½\ \alpha\text{-}Fe_2O_3(s)$, hematite $+ 3H^+$	+(0.06 ± 0.26)	−11.61	3568	–	65.7 ± 1.6	[46], [49]: a, b
$Fe^{3+} + 3/2\ H_2O(l) \rightleftharpoons ½\ \gamma\text{-}Fe_2O_3(s)$, maghemite $+ 3H^+$	−(1.40 ± 0.29)[e]	–	–	–	74.8 ± 1.8	[46]
$Fe^{3+} + 2H_2O(l) \rightleftharpoons \alpha\text{-}FeOOH(s)$, goethite $+ 3H^+$	−(0.16 ± 0.36)[e]	−11.14	3421	–	61.3 ± 2.2	[46], [49]: a, b
$Fe^{3+} + 2H_2O(l) \rightleftharpoons \beta\text{-}FeOOH(s)$, akaganéite $+ 3H^+$	−(0.68 ± 0.47)[e]	–	–	–	70.2 ± 2.4	[46]
$Fe^{3+} + 2H_2O(l) \rightleftharpoons \gamma\text{-}FeOOH(s)$, lepidocrocite $+ 3H^+$	−(1.86 ± 0.44)[e]	–	–	–	72.5 ± 2.2	[46]
$Fe^{3+} + 2H_2O(l) \rightleftharpoons \delta\text{-}FeOOH(s)$, feroxyhie $+ 3H^+$	−(2.18 ± 0.44)	–	–	–	74.3 ± 1.6	[63]
$Fe^{3+} + 3H_2O(l) \rightleftharpoons Fe(OH)_3$(mic), 2-line ferrihydrite $+ 3H^+$	−(3.50 ± 0.40)	–	–	–	80.4 ± 2.2	[49]: $\log_{10}\beta^\circ$, [64]
$Fe^{3+} + 3H_2O(l) \rightleftharpoons Fe(OH)_3$(mic), 6-line ferrihydrite $+ 3H^+$	−(3.00 ± 0.50)	–	–	–	77.2 ± 2.2	[64]
Mixed Fe(II) and Fe(III) iron hydr(oxides)						
$Fe^{2+} + 4/3\ H_2O(l) \rightleftharpoons 1/3\ \alpha\text{-}Fe_3O_4(s)$, magnetite $+ 2H^+ + 1/3\ H_2(g)$	−(12.14 ± 0.15)	−33.7904	6380	4.24014	99.5 ± 0.7	[46], [49]: a, b, c

$\log_{10}\beta^\circ = a + b/T + c\ \ln(T)$.
[a] Value enlisted according to the suggestion of Lemire et al. [46].
[b] Extrapolated from data obtained by Zhao and Pan [55] based on measurements take at $T \geq 60$ °C. Uncertainties overlap.
[c] Value enlisted based on an estimate of Lemire et al. [46].
[d] Computed from $\Delta_r G_m^\circ = -zFU^\circ$, based on $U^\circ = -(0.554 \pm 0.010)$ V [57].
[e] Value enlisted based on $\Delta_f G_m^\circ$ quoted by Lemire et al. [46]. Uncertainties overlap.

temperature and composition dependent phase equilibria of complex (geo)chemical systems [65,66].

The activity coefficients of various ionic species i with formal charge z_i are computed via the extended Debye-Hückel equation in Truesdell-Jones form:

$$log_{10}\gamma_i = \frac{A\cdot[z_i]^2\cdot\sqrt{I}}{1 + B\cdot a\ \sqrt{I}} + b_\gamma \cdot I + log_{10}\frac{x_{i,w}}{X_w}, \quad (1)$$

where b_γ is a semi-empirical parameter ($b_i \sim 0.064$ for NaCl) and $\frac{x_{i,w}}{X_w}$ is the mole fraction of water solvent [51,65]. The Debye-Hückel Limiting Law parameters $A \sim 0.5114$ and $B \sim 0.3288$ are furthermore evaluated at the standard operating temperature $T = 25$ °C and pressure $P = 1$ bar, in line with the conditions of all thermodynamic simulations presented throughout this work. Here, Eq. 1 is applicable for molar ionic strengths, I,

$$I = \frac{1}{2}\sum_{i=1}^{n} c_i z_i^2 \quad (2)$$

ranging from 1 to 2 M, where c_i denotes the respective ionic molar concentration of species i.

In the following section, thermodynamic predictions using the thermodynamic database and the model described in Section 3 are compared to experimental literature data for iron phases in cementitious (Section 2) and other systems. To compute the solubility and speciation of various iron hydr(oxides), Fe(II) and Fe(III) were introduced into pure water at standard temperature and pressure. The pH was varied by adding hydrochloric acid and sodium hydroxide, respectively. For the purpose of comparing the thermodynamic predictions to experimental literature data, for selected cases, other ions and dissolved oxygen were introduced in accordance with the respective experimental conditions reported in the reviewed publications.

4. Thermodynamic predictions and comparison with empirical data

The two oxidation states of iron, Fe(II) and Fe(III), and their respective hydrolysis products contribute to the overall solubility of iron to different extents across the pH range of interest. Their respective contributions, predominance intervals and solubility dictating solid iron (hydr)oxides incorporated in Tables 1 and 2 are briefly discussed within the following sections.

4.1. Aqueous Fe(II) complexes

Under reducing conditions $Fe(OH)_2(s)$ is the dominant solubility dictating Fe(II) oxide. The relative contribution of various Fe(II)

hydrolysis products to the overall Fe(II) solubility is shown in Fig. 2. From the plot of mole fractions (Fig. 2b) it can be recognised that for pH > 8, at least 2 aqueous Fe(II) species significantly contribute to the overall iron solubility of $Fe(OH)_2$(s). For pH > 12, the overall solubility is predominantly dictated by FeO_2H^-, which is often reported in literature with one additional H_2O as $Fe(OH)_3^-$. The overall solubility of $Fe(OH)_2$(s) at pH 13 is relatively low, around $\sim 10^{-7}$ M. For pH lower than 7 (not shown in Fig. 2), Fe^{2+} dominates the solubility, which theoretically increases with decreasing pH with the slope shown in the pH range 7–9 in Fig. 2a. Thus, in acidic as well as deaerated conditions, such as in corrosion pits [67], iron has an extremely high solubility (independently of the presence of chloride).

4.2. Aqueous Fe(III) complexes

The Fe(III)-H_2O system is governed by the formation of five Fe(III) hydrolysis products (Fe^{3+}, $FeOH^{2+}$, FeO_2^-, FeO_2H, FeO^+), three of which (FeO_2^-, FeO_2H, FeO^+) dictate the overall solubility across the alkaline pH range of interest (Fig. 3). Analogous to FeO_2H^- controlling the solubility of Fe(II) at high pH, FeO_2^- (or $Fe(OH)_4^-$, if it is expressed with additional H_2O) is the dominant aqueous Fe(III) complex in highly alkaline environments. Many different iron (hydr)oxides might form depending on temperature, time and the presence of other ions. In most cases, initially well soluble iron hydroxides such as 2-line or 6-line ferrihydrite will precipitate [68,69], which will determine the dissolved iron concentrations during to first hours to months. The more stable phases lepidocrocite, goethite, maghemite or hematite will form after longer reaction times (years to decades) or at higher temperatures. As a consequence of this slow formation of the most stable iron oxides, the aqueous iron concentrations can be expected to decrease with time (at least in the absence of a source for ferric ions).

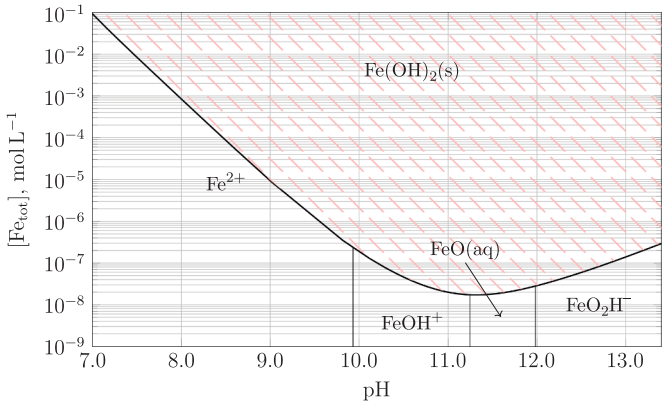

(a) Predominance diagram.

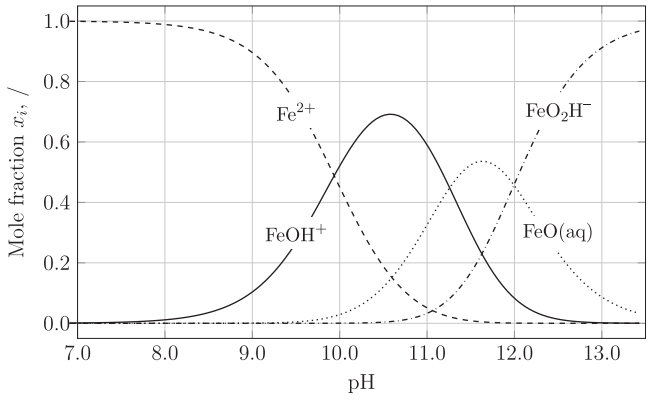

(b) Mole fraction.

Fig. 2. Solubility of Fe(II) vs pH, as controlled by the solubility of $Fe(OH)_2$(s). (a) The total solubility with the predominance interval of all contributing species superimposed. (b) The respective mole fractions x_i and their progression across pH.

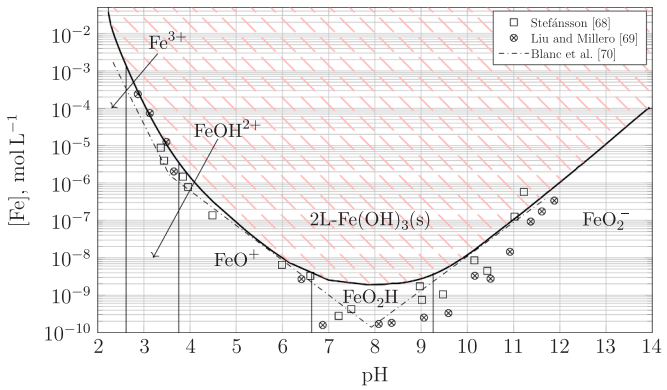

(a) Predominance diagram.

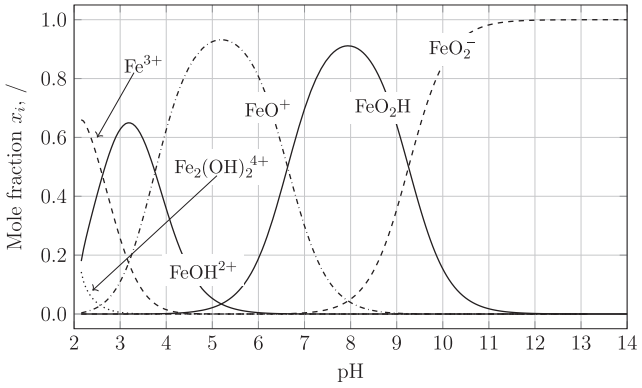

(b) Mole fraction.

Fig. 3. Solubility of Fe(III) vs pH, as controlled by the solubility of 2-line ferrihydrite ($Fe(OH)_3$(s)). (a) Selected experimental data (symbols) in addition to thermodynamic predictions (lines). Aqueous species making the largest contribution to the overall solubility are superimposed on their respective predominant intervals. (b) The respective mole fractions x_i and their progression across pH.

Based on this, Fig. 3 shows the calculated solubility of 2-line $Fe(OH)_3$(s) superimposed by a predominance diagram of the aqueous Fe(III) species, together with selected experimental 2-line $Fe(OH)_3$(s) solubility data. It is evident that selected $\log_{10}\beta^\circ$ (Table 2) agree well with experimental data across the entire pH range considered [68–70]. Note that the contribution of $Fe_3(OH)_4^{5+}$ to the overall solubility of Fe(III) is negligible across the pH interval considered.

4.3. Solid iron oxides

Commonly formed iron oxide phases that constitute corrosion product films and oxide rusts are iron hydroxide ($Fe(OH)_2$(s)), hematite (α-Fe_2O_3(s)), maghemite (γ-Fe_2O_3(s)), goethite (α-FeOOH(s)), akaganéite (β-FeOOH(s)), lepidocrocite (γ-FeOOH(s)), feroxyhite (δ-FeOOH(s)), iron trihydroxide or ferrihydrite ($Fe(OH)_3$(s)) and magnetite (α-Fe_3O_4(s)) [71–74]. In general, they can be distinguished according to their stability in the Fe_2O_3-H_2O system. While metastable variants of FeOOH(s) including lepidocrocite and feroxyhite only form under strongly oxidating conditions [46,75] or are hypothesized to be stable at nanoscale [63], they have been identified to play a significant role in the phase assemblage of secondary, more stable iron oxides [76–78].

For this reason, thermodynamic data and solubility constants of the latter phases are included in this paper to enable a more thorough

comparison of experimentally measured iron concentrations in cementitious systems to those thermodynamically predicted by the competitive precipitation of two or more iron oxides.

4.4. Iron-bearing cementitious phases

Amongst the main constituents of PC clinker,[2] iron is predominantly present in the form of unreacted ferrite ($C_4(A,F)$). It can also exist as ferrihydrite ($Fe(OH)_3(s)$) during the first hours of hydration or bind to siliceous hydrogarnet ($C_3(A,F)S_yH_{6-2y}$ and $C_3FS_yH_{6-2y}$) at longer hydration times [42]. In addition, some Fe(III) might also be present in the form of Fe-hydrotalcite ($M_3F_{0.5}c_{0.5}H_6$), partially replace Al(III) in ettringite ($Ca_6[Al_{1-x}Fe_x(OH)_6]_2(SO_4)_3{\cdot}26H_2O$) and/or monosulfate ($Ca_4[Al_{1-x}Fe_x(OH)_6]_2(SO_4){\cdot}6H_2O$), or be taken up both by C-S-H in the form of Fe(II) or Fe(III) [32,36,37,42,47,79,80]. The ferrihydrite formation during the first hours of hydration [42] indicates the importance of 2-line ferrihydrite ($2l\text{-}Fe(OH)_3(s)$) as a solubility limiting iron bearing phase in accordance with a maximum aqueous iron concentration at early hydration times [35,39,40,42,81]. At later hydration times, ferrihydrite destabilises and converts to hydrogarnet, leading to a decrease of aqueous Fe-concentrations as hydrogarnet is less soluble under high pH conditions. Thus, the solubility limit as dictated by 2-line ferrihydrite represents the upper possible limit of iron concentrations.

4.5. Fe(II) and Fe(III) solubility in cementitious systems

Fig. 4a and b displays the measured iron concentrations across different studies with cements and cement hydrates as presented in Fig. 1. Note that for PC and blended cements, Fe(III) is considered to be the solubility dominating oxidation state of iron. An exception are the cements containing blast furnace slags, which is a by-product of iron production. Due to the reducing conditions in the blast furnace, blast furnace slag contains Fe(0) nanoparticles as well as reduced sulphur species. These reducing conditions remain for an extended period of time even during the life of a concrete structure [44,45].

Aqueous Fe(III) concentrations in equilibrium with synthesised cement hydrate phases in Fig. 4a follow approximately the solubility of lepidocrocite (γ-FeOOH(s)) [36–38]. For a pH $>$ 13, it is furthermore apparent that measurements in PC and blended cements from Andersson et al. [41] and Lothenbach et al. [33] correspond to the $[Fe_{tot}]$ concentration predicted by the solubility of 2- or 6-line $Fe(OH)_3(s)$ (compare Fig. 4b). Somewhat lower iron concentrations were reported by Deschner et al. [34] in PC and PC blended with fly ash, in between the upper and lower solubility limits dictated by 6-line $Fe(OH)_3(s)$ and γ-FeOOH(s). Iron concentrations measured in pore water extracted from slag cement systems [35] appear to be about an order of magnitude higher in iron than the solubility of ferrihydrite (which may be due to the presence of Fe(II) in slag systems). Similarly, for solutions pressed from systems made with PC blended with silica fume, higher iron concentrations were measured below a pH of 12 (x symbols in Fig. 4b) [33].

Iron concentrations measured in the presence of Si and/or carbonates (marked by stars in Fig. 4a) or carbonates (diamonds in Fig. 4a) appear to be clustered together and about an order of magnitude higher than those in its absence. This distinct increase may be due to the formation of some uncharacterised iron-silica and iron-carbonate complexes leading to aqueous iron concentrations higher than those in the absence of Si and/or carbonates. Alternatively, iron oxide precipitation could be impaired in the presence of silica, leading to smaller, structurally disordered crystalline phases in equilibrium with a higher aqueous iron concentration [82].

This phenomenon, if operative, would evidently have a significant impact on the accuracy of thermodynamic modelling approaches

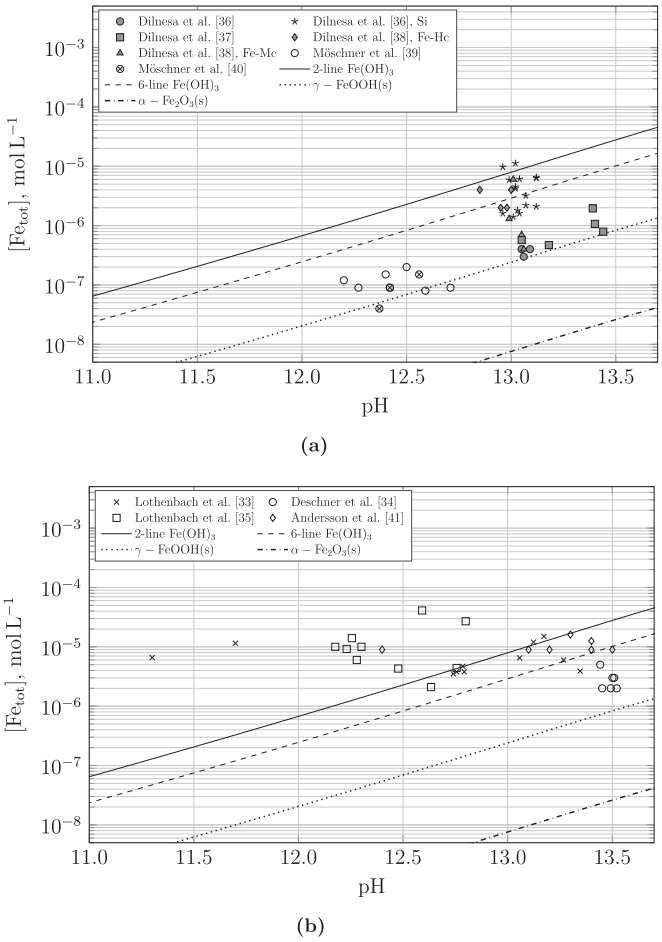

Fig. 4. Total solid 2- and 6-line ferrihydrite ($Fe(OH)_3(s)$), lepidocrocite (γ-FeOOH(s)) and hematite (α-Fe2O3(s)) solubility as predicted by the thermodynamic model, together with selected measured elementary concentrations in cementitious systems versus the pH: Comparison of the model with experimental data (a) in equilibrium with synthesised cementitious phases, (b) pressed from hardened concrete.

predicting the phase assemblage of corrosion products in cementitious systems. Possible implications and limitations of the applicability of equilibrium computations to complex real systems are presented in Section 5.

In Fig. 4, it is noticeable that many aqueous Fe(III) concentrations in equilibrium with synthesised cementitious phases follow the progression of [Fe] as a function of the pH in line with the solubility of γ-FeOOH (s). As evident from Fig. 4b, this trend does not hold true for naturally synthesised cementitious systems due to the multitude of dissolution and uptake mechanisms and due to complex formation prompting elemental pore solution compositions to vary from their expected value.

While the ranges of Fe(III) measurements in cement pore solutions presented appear to be largely in line (with a few exceptions as discussed) with the solubility limits as dictated by 2- and 6-line ferrihydrite (Fig. 4), Fe(II) measurements as illustrated in Fig. 5 can significantly exceed thermodynamically predicted concentrations in equilibrium with $Fe(OH)_2(s)$. Fig. 5 shows the total solubility of $Fe(OH)_2(s)$ as predicted by the thermodynamic model, together with the Fe(II) concentrations measured in NaOH [59], which agrees well with the expected concentrations. In contrast, the Fe(II) concentration determined in cementitious systems [32], that is, in the presence of Ca and Si and other species, were 2–5 orders of magnitude higher, indicating that Ca and Si seem to have a major effect on Fe(II) solubility, either due to the formation of iron complexes or due to hindrance of precipitation,

[2] Cement shorthand notation: C = CaO, A = Al_2O_3, F = Fe_2O_3, S = SiO_2, c = CO_2, s = SO_4, M = MgO and H = H_2O.

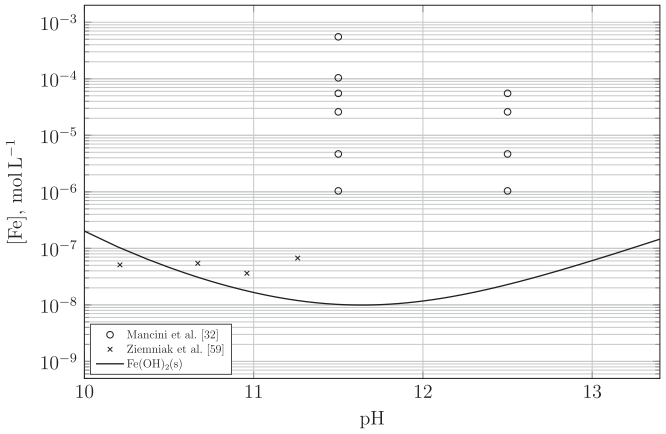

Fig. 5. Total solubility of $Fe(OH)_2(s)$ as predicted by the thermodynamic model, compared with Fe(II) measurements in NaOH solution [59] and in solutions containing also Ca and Si [32].

analogous to the effects of Si and other impurities on the structure of Fe $(OH)_3(s)$ [83,84].

4.6. The effect of chlorides

4.6.1. Aqueous Fe(II) and Fe(III) chloride complexes

Aqueous iron chloride complexes play an important role in the process of self-sustained pitting corrosion. Although the detailed mechanism of passivity breakdown is challenging to observe, there is a consensus emerging that, upon dissolving iron in the form of some iron-chloride complex, Cl^- may be liberated by electrolytic oxidation of that species and hence replenish the corrosion cycle catalytically [27,30,31]. To accurately capture the intricacies of intermediate species formed within that cycle, all iron-chloride complexes characterised to date are included in Tables 1 and 2.

Zhao and Pan [55] investigated the solubility of Fe(II)-chloride complexes assuming the following reaction:

$$Fe^{2+} + nCl^- \leftrightarrow FeCl_n^{2-n} \quad (3)$$

The three obtained solubility constants (i.e., for $n = 1, 2, 4$) are included in the database presented in this work. It must be noted that Zhao and Pan [55] did not report a solubility constant for the tetrahedral complex $FeCl_4^{2-}$ at standard conditions due to its negligible percentage molar contribution at $T < 60$ °C. The corresponding $\log_{10}\beta^\circ$ listed in Table 2 is based on extrapolation of their measurements at 60, 80 and 100 °C, respectively. The thermodynamic calculations for Fe(II) solubility in the presence of chloride are shown in Fig. 6. Comparing this result with Fig. 2, it is concluded that chlorides have no significant effect on the solubility of Fe(II) and that the domains shown in Fig. 2 are not affected.

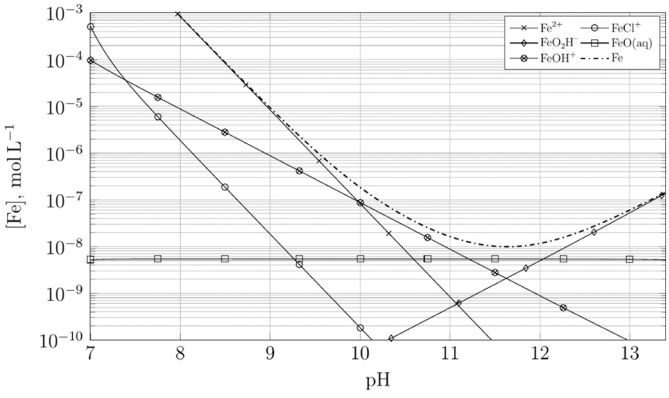

Fig. 6. Solubility of Fe(II) vs pH, as controlled by the solubility of $Fe(OH)_2(s)$ for a background NaCl electrolyte concentration of 100 mM.

Fe(III) chloride complexes follow the recommended solubility constants by Lemire et al. [46]. The only exception to this is $FeCl_4^-$ data, which stems from investigations by Liu et al. [56]. It must be noted that although such Fe(II)/Fe(III) chloride complexes exist, they have a negligible effect on the overall iron solubility. In highly acidic conditions, $FeCl^+$ and $FeCl^{2+}$ reach aqueous concentrations of up to 10^{-4} M, the overall iron solubility is dominated by the respective Fe(II) and Fe (III) hydrolysis products. Similarly, the iron solubility across the pH domain of interest for cementitious systems appears to be entirely dictated by FeO_2H^- and FeO_2^-.

Example theoretical solubility curves for Fe(III) under the effect of chlorides are presented in Fig. 7. The thermodynamic calculations are generally well in agreement with experimental data presented in Fig. 4b. Overall, the data shown in Figs. 6 and 7 illustrate that chlorides have a negligible effect on the solubility of both Fe(II) and Fe(III).

4.6.2. Fe(II) and Fe(III) chloride solids

In hindsight to the discussion on chloro-complexation and its effect on the overall solubility of iron in cementitious systems, thermodynamic data of $GR(Cl^-)$ was added to Tables 1 and 2. Green rusts (GR) form as an intermediate product during the oxidation of $Fe(OH)_2$ and consists of brucite-like $Fe(OH)_2$ layers, where the partial oxidation of Fe(II) to Fe (III) results in a positive charge. This charge is compensated by anions

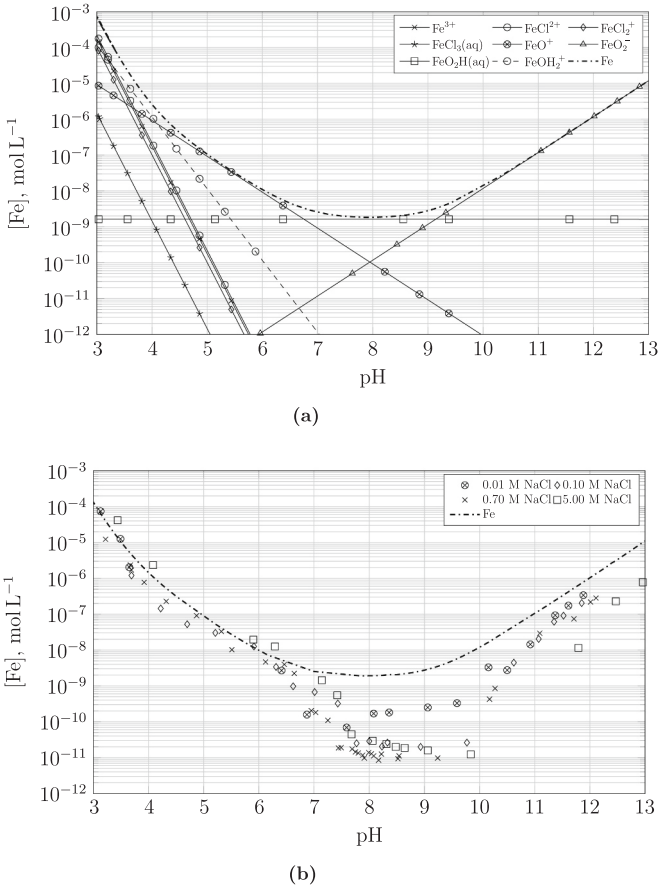

Fig. 7. Effect of chlorides on the Fe(III) solubility; thermodynamic predictions of the solubility of 2-line ferrihydrite ($Fe(OH)_3(s)$, dashed line), (a) together with the modelled contributing aqueous Fe(III) species vs. pH for a background NaCl electrolyte concentration of 100 mM; (b) compared to the experimental values obtained by Liu and Millero [69] for varying electrolyte concentrations of 0.01–5.00 M NaCl versus the pH.

and water molecules present in the interlayer. GR(Cl^-) is a mixed Fe(II)-Fe(III)-hydroxide solid and belongs to the structural group of pyroaurite-sjögrenite layered hydroxides [58]. In contrast to carbonate and sulfate green rusts, available thermodynamic parameters for GR(Cl^-) are sparse. Refait and Génin [58] measured a chemical potential of $U^\circ = -0.554 \pm 0.01$ V for the oxidation reaction.

$$Fe(OH)_2(s) + Cl^- + H^+ + nH_2O(l) \leftrightarrow (Fe^{3+})(Fe^{2+})_3(OH)_8Cl{\cdot}nH_2O(s) + {}^1/_2 H_2(g). \quad (4)$$

This value was corrected to zero ionic strength by Lemire et al. [46]: $U^\circ = -0.552 \pm 0.012$ V resulting in a $\log_{10} K^\circ(298.15\ K) = (9.32 \pm 0.35)$ and $\Delta_f G_m^\circ(GR(Cl^-)) = -2639 \pm 2$ kJ mol^{-1}, which was accepted in the present study. Bourdoiseau et al. [85] re-evaluated the available data obtaining suggesting a $\Delta_f G_m^\circ(GR(Cl^-)) \sim -2620$ kJ mol^{-1}; the significant variation in the thermodynamic data for green rust is related to the high uncertainty of the Gibbs free energy of solid $Fe(OH)_2$.

Sagoe-Crentsil and Glasser [30] indicated the possibility that GR (Cl^-) could dictate the overall iron solubility in systems containing, Fe (II), Fe(III) and chloride, as they observed its formation in their experiments, where they oxidised Fe(0) in the presence of chloride at high pH values in an electrolyte containing 0.88 g NaOH, 3.45 g KOH and 0.48 g $Ca(OH)_2$. The authors [30] suggested that the formation of an aqueous iron chloride complex can explain the strongly increased iron concentrations in the presence of chloride shown in Fig. 8. However, the suggested aqueous iron chloride complexes seems not very probable, as i) other available studies [46,69] showed no significant effect of chloride on Fe(II) and Fe(III) solubility at high pH values as discussed above and ii) as the presence of only 15 mM of chloride in solution can hardly increase the total iron concentration from ≪1 mM to 160 mM (Fig. 8) based on aqueous complex formation.

As an alternative explanation for the observations reported by Sagoe-Crentsil and Glasser [30] we suggest that the formation of nano-sized GR (Cl^-) particles could explain the strongly increased iron concentration in solution. Depending on the filtration procedure (which is not specified in [30]), nano-sized GR(Cl^-) particles could have remained in the suspension analysed leading to an apparent very strong increase of total Fe found as illustrated in Fig. 8. This hypothesis can be tested by thermodynamically modelling the sum of soluble iron species and GR(Cl^-) rust as a function of chloride concentration in the solution. The result of such a model calculation is shown in Fig. 8. The figure reveals excellent agreement between the experimental data and the calculation. Thus, it appears likely that the experimentally quantified "soluble" iron by Sagoe-Crentsil and Glasser [30] included GR(Cl^-), which may have been present as nano-sized particles in the suspension. Experimental uncertainties overlap the steady-state total iron concentrations for [Cl^-] above the reported stepwise increment at ~15 mM.

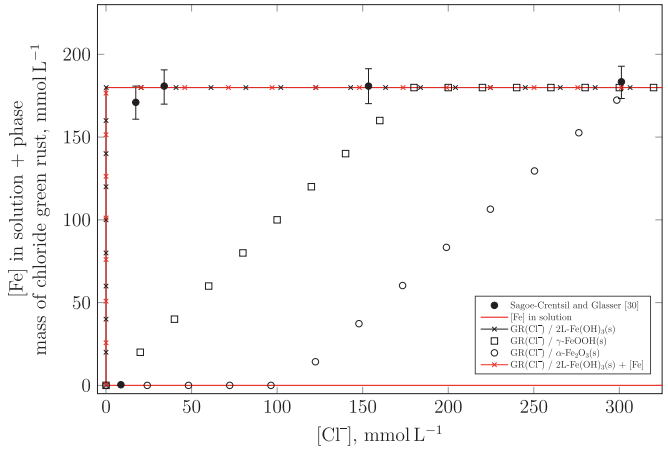

Fig. 8. Total solubility of GR(Cl^-) as measured by Sagoe-Crentsil and Glasser [30], together with the solubility of GR(Cl^-) as predicted by thermodynamic calculations for chloride electrolyte concentrations varying from 0 to 350 mM at $T = 25$ °C. The performed thermodynamic simulations mimic the electrolytic pore fluid composition of Sagoe-Crentsil and Glasser [30], including 0.88 g NaOH, 3.45 g KOH and 0.48 g $Ca(OH)_2$. The experimentally measured and calculated pH ~ 13 are virtually identical.

The onset of the sharp increase in the amount of GR(Cl^-), as apparent from Fig. 8, depends on the type of iron (hydr)oxides that form in addition to GR(Cl^-). Allowing (in the thermodynamic model) for the simultaneous precipitation of well soluble 2-line $Fe(OH)_3$(s), the phase mass of GR(Cl^-) is calculated to increase at [Cl^-] ≈ 0.5 mM (x symbols in Fig. 8). Higher stability oxides such as lepidocrocite (γ-FeOOH(s)) or hematite (α-Fe_2O_3(s)) cause a more gradual increase towards the limiting GR(Cl^-) concentration of ~180 mM (circles in Fig. 8). Thermodynamic modelling allowing for the formation of GR(Cl^-) and goethite (α-FeOOH(s)), however, predict the exclusive formation of the latter, with no GR(Cl^-) formed up to 2 M chloride. The implications of these competitively forming species is discussed in the next section.

4.6.3. Stability domains of green rust and magnetite

The calculation of saturation index $SI = \log_{10}(IAP/K_{sp})$ allows to independently assess which solid is expected to form from solution. K_{sp} corresponds to the solubility product, while the ion activity product, $IAP = \prod_{i=1}^{n}\{X_i\}^{\nu_i}$ can be calculated from aqueous concentrations. A negative saturation index, i.e. $K_{sp} > IAP$, implies the dissolution of a solid phase, a positive saturation index indicates its tendency to form. As increments in the aqueous chloride concentration promote the formation of chloride-bearing phases ($X_i = Cl^-$), it is therefore of interest to compute [Cl^-] at which magnetite ceases to have a higher proclivity to form than GR(Cl^-). Fig. 9 illustrates the ratio of saturation indices $SI_{GR(Cl^-)}/SI_{Fe_3O_4(s)}$ and its progression with [Cl^-].

The threshold chloride concentration above which GR(Cl^-) is preferentially stabilized appears to be highly sensitive to changes in the dissolved oxygen content as well as the pH. Fig. 10 displays the locus of chloride concentrations marking $SI_{GR(Cl^-)} = SI_{Fe3O4(s)}$for a range of pH and $[O_2]_{added}/[Fe(II)]$ values.

In the absence of dissolved oxygen, reference chloride concentrations required to stabilise GR(Cl^-) are consistently <25 mM in the interval of pH [11.7,12.5]. Findings are consistent with experimental measurements confirming the formation of magnetite for [NaCl] = 10 mM and $[O_2(aq)] = 0.10$ mg L^{-1} [86]. For any pH out of these bounds, the chloride concentration required to achieve preferential stabilisation of GR(Cl^-) over magnetite increases drastically. This trend holds true for successively higher $[O_2]_{added}$ to [Fe(II)] ratios. The amount of oxygen does not affect the amount of chloride required to stabilise GR(Cl^-) for a pH < 11.5. In contrast, the intermediary plateauing region is shifted upwards to 26, 36 and 44 mM for ratio $[O_2]_{added}/[Fe(II)] = 1$, 3 and 5%,

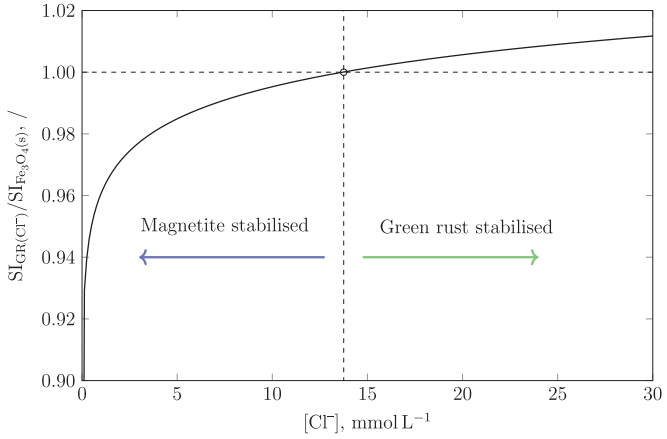

Fig. 9. Ratio of saturation indices $SI = \log_{10}(IAP/K_{sp})$ of GR(Cl^-) and magnetite (α-Fe_3O_4(s)) as a function of aqueous chloride concentration.

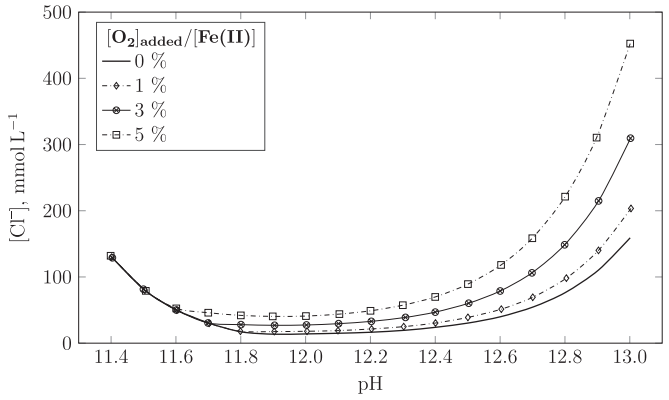

Fig. 10. Locus of chloride concentrations based on thermodynamic predictions, marking the transition between GR(Cl^-) and magnetite (αFe_3O_4(s)) stability as a function of the $[O_2]_{added}$ to [Fe(II)] ratio and the pH.

respectively. At pH = 13, the same increments in the added oxygen content shift the transition chloride concentration to 200, 310 and 450 mM.

The effect of both the dissolved oxygen concentration and the pH on the stability regime of GR(Cl^-) rust has major consequences on the modelling of corrosion product transport and formation.

5. Further discussion

5.1. Kinetics aspects and nucleation growth

Thermodynamic energy minimisation routines do, by default, not accommodate for the underlying reaction mechanism leading to the formation of the most stable phase. A holistic model that accurately captures the formation of various corrosion products over time must therefore consider thermodynamic expert judgement on the crystalline phases that could form as well as kinetic effects.

This becomes particularly apparent in precipitation experiments, when Fe(0) oxidises in contact with the pore solution of a cement. Liu and Millero [69] investigated the precipitation of iron hydroxide (2-line Fe(OH)3(s)) in the presence of varying NaCl concentrations. As illustrated by Fig. 11, approaching Fe(III) concentration levels close to equilibrium may take considerable time, such as in the range of a few hours to weeks. Moreover, it is apparent that equilibrium is approached more slowly under both acidic and alkaline conditions with respect to pH neutral conditions. This kinetic mechanism may thus cause a significantly higher portion of iron to remain mobile in the aqueous phase in cementitious systems. Assuming a sufficiently high diffusive and migrative driving force, $Fe(OH)_3$(s) precipitation can be regarded as a slow process, even at sufficiently supersaturated solutions, compared to the rate of mass transfer distributing mobile iron species across the pore network [87].

The formation of thermodynamically stable solid phases including commonly identified corrosion products is usually described by classical nucleation and growth theory [88]. Recent studies however propose the precipitation of some secondary crystalline phase via the formation and aggregation of primary, metastable intermediates [76–78]. Soltis et al. [76] investigated the mineral phase transformation from 2-line ferrihydrite to hematite. Measurements of dissolved Fe(III) concentration indicated a second-order kinetics for the consumption of aqueous Fe(III). These observations appear to concur with a proposed hematite growth mechanism driven by the formation of akaganéite nanoparticle as precursors [77] and the formation of magnetite via co-precipitation of Fe(II) and Fe(III) phases in alkaline solutions [78]. It is furthermore speculated that similar mechanisms are applicable to the growth of secondary phases other than hematite and magnetite [77,78]. Fe(III) concentrations are therefore expected to be significantly higher during the precipitation process than the concentration in equilibrium with the precipitating corrosion products. By analogous reasoning, considering the ample deviations in measured and thermodynamically predicted Fe (II) concentrations presented in Fig. 5, it cannot be excluded that Fe $(OH)_2$(s) precipitation is subjected to an equally intricate and time consuming kinetic mechanism.

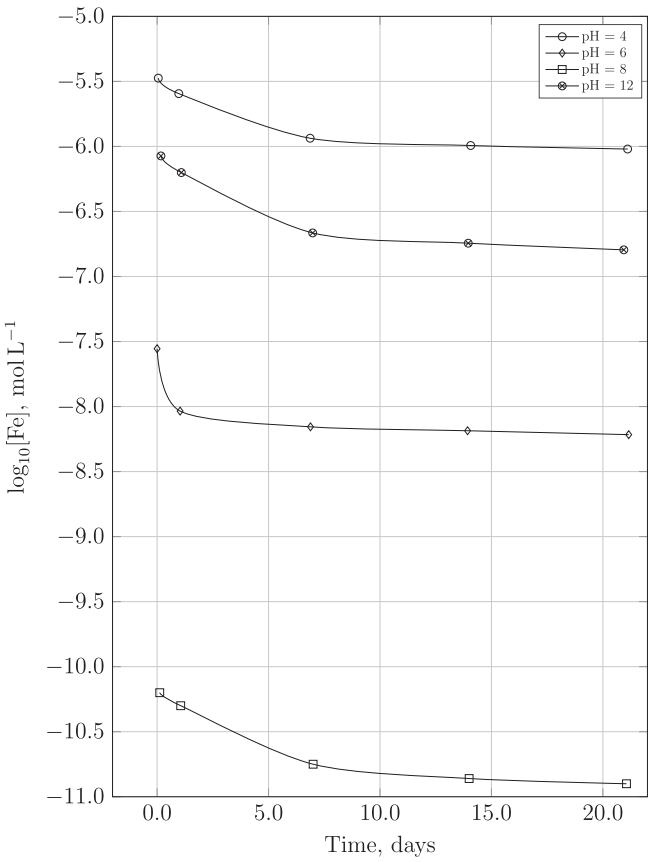

Fig. 11. Fe(III) concentrations in 0.7 M NaCl at T = 25 °C as a function of time across various pH, adapted from Liu and Millero [69].

5.2. The possible role of chlorides in corrosion

In situations of corroding steel in concrete, there is a constant supply of ferrous ions at the metal surface. This is in contrast to unreinforced concrete, where iron may stem from sources such as raw materials (cement, aggregates) and is generally found in a state achieved after relatively long equilibrium times such as the oxidated state. The very high solubility of Fe(II) in cementitious systems can thus play an important role in the corrosion process itself as well as in the subsequent transport and precipitation of corrosion products in the cementitious matrix, ultimately leading to damage such as cracking and spalling.

In an attempt to explore the effect of chlorides on corrosion product formation and the corrosion process, thermodynamic simulations show that GR(Cl^-) rust may indeed be an intermediate solubility limiting iron solid at alkaline pH. One may hypothesize that GR(Cl^-) formation *temporarily* increases the amount of iron (both as aqueous Fe species and as nano crystallite particles) present in the aqueous phase, hence mediating iron transport and therefore corrosion product formation distant from the steel-concrete interface. It can furthermore not be excluded that iron oxide aggregation steps similar to those observed to precede hematite and magnetite phase formation also involve GR(Cl^-). Chloro-complexation and subsequent oxidation would hence play a vital role in the catalytic cycle of iron electro-dissolution [30]. Based on experimental data at disposal, it is clearly difficult to ascertain a time

frame across which GR(Cl^-) remains stable in real cementitious systems. This stresses the need for further experimental work, both on the thermodynamic stability of GR(Cl^-) as well as its kinetic mechanism of formation and dissolution.

5.3. Future research challenges

As became apparent from the literature review presented in Section 2, experimental studies investigating the sensitivity of aqueous iron concentration and time-dependent corrosion product formation both for aqueous and cementitious systems is scarce. To address open questions deduced from the discussion presented in this section, a number of research challenges have been identified.

- To enable a quantitative comparison between transport and precipitation of aqueous iron species, kinetic rate equations accommodating for changes in the pH [69], reactant stoichiometry and geometry [89] of the precipitated solubility limiting corrosion product must be developed.
- Given the scarcity of time-dependent iron concentration measurements, it is challenging to (i) obtain kinetic rate equation parameters accounting for the multitude of influencing factors identified and (ii) deduce a non-ambiguous sequence of kinetic steps leading up to the precipitation of the most thermodynamically feasible corrosion product. Empirical measurements presented in this paper must hence be complemented by a range of experimental investigations that systematically assess the progression of aqueous iron concentration over time.
- The kinetics of Fe(II) oxidation is well described in the acidic to mildly alkaline conditions [90]. To assess the feasibility of chloro-complexation in real systems and the availability of Fe(II) and Fe(III) in ratios allowing for the formation of GR(Cl^-), existing rate equations for $d[Fe(II)]/dt$ must be extended into the alkaline pH relevant for cementitious systems.
- The possibility of the presence of nano-sized GR(Cl^-) particle and their effect on the transport of iron away from the steel surface should be further investigated.

6. Conclusions

Based on updating a thermodynamic database to comprise state-of-the-art data for all aqueous iron species and solid oxides, and comparing related thermodynamic calculations to compiled empirical data on the elemental composition of pore solutions from cementitious systems, the following major conclusions can be drawn:

1. Literature data on aqueous iron concentrations and time-dependent formation of solid iron phases is scarce, particularly for cementitious environments. However, the available data indicates that the presence of cementitious phases introduces significant complexity and influences the solubility and speciation of iron with respect to other aqueous systems.
2. Under oxidizing conditions, Fe(III) concentrations in cement pore solutions appear to be generally in agreement with the solubility limits expected from by 2- and 6-line ferrihydrite, or to deviate from this by maximum 1 order of magnitude, such as in the presence of Si and/or carbonates.
3. The solubility of Fe(II) (hydr)oxides, on the other hand, can in cementitious systems exceed the solubility expected from thermodynamic predictions by several orders of magnitude. Literature data suggests that this may be due to the formation of so far unknown iron complexes or due to (kinetic) hindrance of precipitation.
4. Thermodynamic considerations suggest that chlorides do not significantly increase the solubility of iron. However, at a pH range around 12, small amounts of chloride are sufficient to stabilise GR (Cl^-). From comparing these thermodynamic considerations with experimental literature data, it seems probable that GR(Cl^-) may initially form, e.g. as nano-sized particles that, as they stay in suspension, can be available for transport through the cementitious matrix, until they may be converted to other phases and precipitate.
5. Since the speciation of iron in cementitious systems has effects on reinforcing steel corrosion and related damage processes on various levels, further research is needed to close the highlighted gaps in the literature with respect to the solubility of Fe(II) and Fe(III) (hydr) oxides in cementitious environments, both with and without chlorides, as well as the kinetics of formation and transformation of different phases.

CRediT authorship contribution statement

Fabio E. Furcas: Conceptualization, Investigation, Formal analysis, Visualization, Writing – original draft. **Barbara Lothenbach:** Conceptualization, Formal analysis, Writing – review & editing, Supervision. **O. Burkan Isgor:** Conceptualization, Writing – review & editing, Supervision. **Shishir Mundra:** Writing – review & editing. **Zhidong Zhang:** Writing – review & editing. **Ueli M. Angst:** Conceptualization, Writing – review & editing, Supervision, Funding acquisition.

Declaration of competing interest

The authors declare that they have no known competing financial interests or personal relationships that could have appeared to influence the work reported in this paper.

Acknowledgements

The authors are grateful to the European Research Council (ERC) for the financial support provided under the European Union's Horizon 2020 research and innovation program (grant agreement no. 848794). Additionally, we would like to thank Dr. Andreas Thoenen from the Paul Scherrer Institute (PSI) in Switzerland for the valuable discussion on the selection of thermodynamic data for iron compounds. The support from ETH Zurich internal funding and NSF CMMI 1728358 helped enable the collaboration between ETH Zurich and Oregon State University.

References

[1] C. Hansson, The impact of corrosion on society, Metall. Mater. Trans. A 42 (2011) 2952–2962.
[2] D. Yilmaz, U. Angst, Korrosionsbedingte Kosten an Ingenieurbauwerken im Schweizer Straßennetz, Beton Stahlbetonbau 115 (2020) 448–458.
[3] S. Kranc, A.A. Sagüés, Detailed modeling of corrosion macrocells on steel reinforcing in concrete, Corros. Sci. 43 (2001) 1355–1372.
[4] M. Brem, Numerische Modellierung der Korrosion in Stahlbetonbauten: Anwendung der Boundary Element Methode, ETH Zurich, 2004.
[5] O.B. Isgor, A.G. Razaqpur, Modelling steel corrosion in concrete structures, Mater. Struct. 39 (2006) 291–302.
[6] O.B. Isgor, A.G. Razaqpur, Advanced modelling of concrete deterioration due to reinforcement corrosion, Can. J. Civ. Eng. 33 (2006) 707–718.
[7] M. Raupach, Models for the propagation phase of reinforcement corrosion — an overview, Mater. Corros. 57 (2006) 605–613.
[8] J. Warkus, M. Raupach, Numerical modelling of macrocells occurring during corrosion of steel in concrete, Mater. Corros. 59 (2008) 122–130.
[9] U.M. Angst, Challenges and opportunities in corrosion of steel in concrete, Mater. Struct. 51 (2018) 1–20.
[10] D.A. Hausmann, Steel corrosion in concrete. How does it occur? Mater Protect 6 (1967) 19–23.
[11] C. Alonso, M. Castellote, C. Andrade, Chloride threshold dependence of pitting potential of reinforcements, Electrochim. Acta 47 (2002) 3469–3481.
[12] Y. Cao, C. Gehlen, U. Angst, L. Wang, Z. Wang, Y. Yao, Critical chloride content in reinforced concrete — an updated review considering Chinese experience, Cem. Concr. Res. 117 (2019) 58–68.
[13] M. Hamada, Neutralization (carbonation) of concrete and corrosion of reinforcing steel, in: 5th Int. Symp. on Cement Chemistry, The Cement Association of Japan, Tokyo, 1968, pp. 343–369.
[14] U. Angst, F. Moro, M. Geiker, S. Kessler, H. Beushausen, C. Andrade, J. Lahdensivu, A. Köliö, K.-I. Imamoto, S. von Greve-Dierfeld, Corrosion of steel in carbonated concrete: mechanisms, practical experience, and research priorities — a critical review by RILEM TC 281-CCC, RILEM Techn. Lett. 5 (2020) 85–100.

[15] N. Berke, M.C. Hicks, Predicting chloride profiles in concrete, Corrosion 50 (1994) 234–239.
[16] E. Samson, J. Marchand, J. Beaudoin, Describing ion diffusion mechanisms in cement-based materials using the homogenization technique, Cem. Concr. Res. 29 (1999) 1341–1345.
[17] T. Luping, J. Gulikers, On the mathematics of time-dependent apparent chloride diffusion coefficient in concrete, Cem. Concr. Res. 37 (2007) 589–595.
[18] O.B. Isgor, W.J. Weiss, A nearly self-sufficient framework for modelling reactive-transport processes in concrete, Mater. Struct. 52 (2019) 1–17.
[19] C. Page, J. Havdahl, Electrochemical monitoring of corrosion of steel in microsilica cement pastes, Mater. Struct. 18 (1985) 41–47.
[20] G. Glass, C. Page, N. Short, Factors affecting the corrosion rate of steel in carbonated mortars, Corros. Sci. 32 (1991) 1283–1294.
[21] U. Angst, B. Elsener, C.K. Larsen, Ø. Vennesland, Chloride induced reinforcement corrosion: rate limiting step of early pitting corrosion, Electrochim. Acta 56 (2011) 5877–5889.
[22] M. Stefanoni, U.M. Angst, B. Elsener, Kinetics of electrochemical dissolution of metals in porous media, Nat. Mater. 18 (2019) 942–947.
[23] K. Vu, M.G. Stewart, J. Mullard, Corrosion-induced cracking: experimental data and predictive models, ACI Struct. J. 102 (2005) 719.
[24] V. L'Hostis, A. Millard, S. Perrin, E. Burger, D. Neff, P. Dillmann, Modelling the corrosion-induced cracking of reinforced concrete structures exposed to the atmosphere, Mater. Corros. 62 (2011) 943–947.
[25] U. Angst, B. Elsener, A. Jamali, B. Adey, Concrete cover cracking owing to reinforcement corrosion — theoretical considerations and practical experience, Mater. Corros. 63 (2012) 1069–1077.
[26] A. Jamali, U. Angst, B. Adey, B. Elsener, Modeling of corrosion-induced concrete cover cracking: a critical analysis, Constr. Build. Mater. 42 (2013) 225–237.
[27] H. Wong, Y. Zhao, A. Karimi, N. Buenfeld, W. Jin, On the penetration of corrosion products from reinforcing steel into concrete due to chloride-induced corrosion, Corros. Sci. 52 (2010) 2469–2480.
[28] T. Marcotte, C. Hansson, Corrosion products that form on steel within cement paste, Mater. Struct. 40 (2007) 325–340.
[29] S.J. Jaffer, C.M. Hansson, Chloride-induced corrosion products of steel in cracked-concrete subjected to different loading conditions, Cem. Concr. Res. 39 (2009) 116–125.
[30] K. Sagoe-Crentsil, F.P. Glasser, Green rust", iron solubility and the role of chloride in the corrosion of steel at high pH, Cem. Concr. Res. 23 (1993) 785–791.
[31] H. DorMohammadi, Q. Pang, P. Murkute, L. Árnadóttir, O.B. Isgor, Investigation of chloride-induced depassivation of iron in alkaline media by reactive force field molecular dynamics, npj Mater. Degrad. 3 (2019) 1–11.
[32] A. Mancini, E. Wieland, G. Geng, B. Lothenbach, B. Wehrli, R. Dähn, Fe (II) interaction with cement phases: method development, wet chemical studies and X-ray absorption spectroscopy, J. Colloid Interface Sci. 588 (2021) 692–704.
[33] B. Lothenbach, D. Rentsch, E. Wieland, Hydration of a silica fume blended low-alkali shotcrete cement, Phys. Chem. Earth A/B/C 70 (2014) 3–16.
[34] F. Deschner, B. Lothenbach, F. Winnefeld, J. Neubauer, Effect of temperature on the hydration of Portland cement blended with siliceous fly ash, Cem. Concr. Res. 52 (2013) 169–181.
[35] B. Lothenbach, G. Le Saout, M.B. Haha, R. Figi, E. Wieland, Hydration of a low-alkali CEM III/B-SiO_2 cement (LAC), Cem. Concr. Res. 42 (2012) 410–423.
[36] B.Z. Dilnesa, B. Lothenbach, G. Renaudin, A. Wichser, D. Kulik, Synthesis and characterization of hydrogarnet $Ca_3(Al_xFe_{-x})_2(SiO_4)_y(OH)_{4(3-y)}$, Cem. Concr. Res. 59 (2014) 96–111.
[37] B.Z. Dilnesa, B. Lothenbach, G. Renaudin, A. Wichser, E. Wieland, Stability of monosulfate in the presence of iron, J. Am. Ceram. Soc. 95 (2012) 3305–3316.
[38] B. Dilnesa, B. Lothenbach, G. Le Saout, G. Renaudin, A. Mesbah, Y. Filinchuk, A. Wichser, E. Wieland, Iron in carbonate containing AFm phases, Cem. Concr. Res. 41 (2011) 311–323.
[39] G. Möschner, B. Lothenbach, J. Rose, A. Ulrich, R. Figi, R. Kretzschmar, Solubility of Fe-ettringite ($Ca_6[Fe(OH)_6]_2(SO_4)_3{\cdot}26H_2O$), Geochim. Cosmochim. Acta 72 (2008) 1–18.
[40] G. Möschner, B. Lothenbach, F. Winnefeld, A. Ulrich, R. Figi, R. Kretzschmar, Solid solution between Al-ettringite and Fe-ettringite ($Ca_6[Al_{1-x}Fe_x(OH)_6]_2(SO_4)_3{\cdot}26H_2O$), Cem. Concr. Res. 39 (2009) 482–489.
[41] K. Andersson, B. Allard, M. Bengtsson, B. Magnusson, Chemical composition of cement pore solutions, Cem. Concr. Res. 19 (1989) 327–332.
[42] B. Dilnesa, E. Wieland, B. Lothenbach, R. Dähn, K. Scrivener, Fe-containing phases in hydrated cements, Cem. Concr. Res. 58 (2014) 45–55.
[43] B. Lothenbach, K. Scrivener, R. Hooton, Supplementary cementitious materials, Cem. Concr. Res. 41 (2011) 1244–1256.
[44] S.A. Bernal, V. Rose, J.L. Provis, The fate of iron in blast furnace slag particles during alkali-activation, Mater. Chem. Phys. 146 (2014) 1–5.
[45] A. Mancini, B. Lothenbach, G. Geng, D. Grolimund, D. Sanchez, S. Fakra, R. Dähn, B. Wehrli, E. Wieland, Iron speciation in blast furnace slag cements, Cem. Concr. Res. 140 (2021), 106287.
[46] R.J. Lemire, U. Berner, C. Musikas, D.A. Palmer, P. Taylor, O. Tochiyama, J. Perrone, Chemical Thermodynamics of iron – Part 1 – Chemical Thermodynamics, Nuclear Energy Agency of the OECD (NEA), 2013.
[47] A. Mancini, E. Wieland, G. Geng, R. Dähn, J. Skibsted, B. Wehrli, B. Lothenbach, Fe (III) uptake by calcium silicate hydrates, Appl. Geochem. 113 (2020), 104460.
[48] R. Lemire, P. Taylor, H. Schlenz, D. Palmer, Chemical Thermodynamics of Iron – Part 2 – Chemical Thermodynamics, Nuclear Energy Agency of the OECD (NEA), 2020.
[49] P.L. Brown, C. Ekberg, Hydrolysis of Metal Ions, John Wiley & Sons, 2016.
[50] B. Lothenbach, D.A. Kulik, T. Matschei, M. Balonis, L. Baquerizo, B. Dilnesa, G. D. Miron, R.J. Myers, Cemdata18: a chemical thermodynamic database for hydrated Portland cements and alkali-activated materials, Cem. Concr. Res. 115 (2019) 472–506.
[51] H.C. Helgeson, D.H. Kirkham, G.C. Flowers, Theoretical prediction of the thermodynamic behavior of aqueous electrolytes by high pressures and temperatures; IV, calculation of activity coefficients, osmotic coefficients, and apparent molal and standard and relative partial molal properties to 600 °C and 5 kb, Am. J. Sci. 281 (1981) 1249–1516.
[52] T. Thoenen, W. Hummel, U. Berner, E. Curti, The PSI/Nagra Chemical Thermodynamic Database 12/07, PSI Report 14-04, PSI, Villigen, Switzerland, 2014.
[53] R.A. Robie, B.S. Hemingway, Thermodynamic Properties of Minerals and Related Substances at 298.15 K and 1 Bar (105 Pascals) Pressure and at Higher Temperatures, US Government Printing Office, 1995.
[54] R. Mesmer, C. Baes, The Hydrolysis of Cations, John Wiley & Sons, New York, London, Sydney, Toronto, 1976.
[55] R. Zhao, P. Pan, A spectrophotometric study of Fe (II)-chloride complexes in aqueous solutions from 10 to 100 °C, Can. J. Chem. 79 (2001) 131–144.
[56] W. Liu, B. Etschmann, J. Brugger, L. Spiccia, G. Foran, B. McInnes, UV–Vis spectrophotometric and XAFS studies of ferric chloride complexes in hyper-saline LiCl solutions at 25–90 °C, Chem. Geol. 231 (2006) 326–349.
[57] P. Refait, J.-M. Génin, The oxidation of ferrous hydroxide in chloride-containing aqueous media and Pourbaix diagrams of green rust one, Corros. Sci. 34 (1993) 797–819.
[58] P. Refait, M. Abdelmoula, J.-M. Génin, Mechanisms of formation and structure of green rust one in aqueous corrosion of iron in the presence of chloride ions, Corros. Sci. 40 (1998) 1547–1560.
[59] S. Ziemniak, M. Jones, K. Combs, Magnetite solubility and phase stability in alkaline media at elevated temperatures, J. Solut. Chem. 24 (1995) 837–877.
[60] H. Lutz, H. Möller, M. Schmidt, Lattice vibration spectra. Part LXXXII. Brucite-type hydroxides $M(OH)_2$ (M = Ca, Mn, Co, Fe, Cd) — IR and Raman spectra, neutron diffraction of $Fe(OH)_2$, J. Mol. Struct. 328 (1994) 121–132.
[61] J. Majzlan, B.E. Lang, R. Stevens, A. Navrotsky, B.F. Woodfield, J. Boerio-Goates, Thermodynamics of Fe oxides: part I. Entropy at standard temperature and pressure and heat capacity of goethite (α-FeOOH), lepidocrocite (γ-FeOOH), and maghemite (γ-Fe_2O_3), Am. Mineral. 88 (2003) 846–854.
[62] J.E. Post, V.F. Buchwald, Crystal structure refinement of akaganéite, Am. Mineral. 76 (1991) 272–277.
[63] J. Majzlan, C.B. Koch, A. Navrotsky, Thermodynamic properties of feroxyhyte (δ′-FeOOH), Clay Clay Miner. 56 (2008) 526–530.
[64] J. Majzlan, A. Navrotsky, U. Schwertmann, Thermodynamics of iron oxides: part III. Enthalpies of formation and stability of ferrihydrite (~$Fe(OH)_3$), schwertmannite (~$FeO(OH)_{3/4}(SO_4)_{1/8}$), and ε-$Fe_2O_3$, Geochim. Cosmochim. Acta 68 (2004) 1049–1059.
[65] D.A. Kulik, T. Wagner, S.V. Dmytrieva, G. Kosakowski, F.F. Hingerl, K. V. Chudnenko, U.R. Berner, GEM-Selektor geochemical modeling package: revised algorithm and GEMS3K numerical kernel for coupled simulation codes, Comput. Geosci. 17 (2013) 1–24.
[66] T. Wagner, D.A. Kulik, F.F. Hingerl, S.V. Dmytrieva, GEM-Selektor geochemical modeling package: TSolMod library and data interface for multicomponent phase models, Can. Mineral. 50 (2012) 1173–1195.
[67] L. Bertolini, B. Elsener, P. Pedeferri, E. Redaelli, R. Polder, Corrosion of Steel in Concrete, Wiley-Vch, Weinheim, Germany, 2013.
[68] A. Stefánsson, Iron (III) hydrolysis and solubility at 25 C, Environ. Sci. Technol. 41 (2007) 6117–6123.
[69] X. Liu, F.J. Millero, The solubility of iron hydroxide in sodium chloride solutions, Geochim. Cosmochim. Acta 63 (1999) 3487–3497.
[70] P. Blanc, A. Lassin, P. Piantone, M. Azaroual, N. Jacquemet, A. Fabbri, E. C. Gaucher, Thermoddem: a geochemical database focused on low temperature water/rock interactions and waste materials, Appl. Geochem. 27 (2012) 2107–2116.
[71] T.D. Marcotte, Characterization of Chloride-induced Corrosion Products that Form in Steel-reinforced Cementitious Materials, University of Waterloo, Waterloo, Ontario, Canada, 2001.
[72] S.J. Oh, D. Cook, H. Townsend, Characterization of iron oxides commonly formed as corrosion products on steel, Hyperf. Interact. 112 (1998) 59–66.
[73] R.A. Antunes, I. Costa, D.L.A.D. Faria, Characterization of corrosion products formed on steels in the first months of atmospheric exposure, Mater. Res. 6 (2003) 403–408.
[74] N.A. North, Corrosion products on marine iron, Stud. Conserv. 27 (1982) 75–83.
[75] F. Chukhrov, B. Zvyagin, A. Gorshkov, L. Yermilova, V. Korovushkin, Y. S. Rudnitskaya, N.Y. Yakubovskaya, Feroxyhyte, a new modification of FeOOH, Int. Geol. Rev. 19 (1977) 873–890.
[76] J.A. Soltis, J.M. Feinberg, B. Gilbert, R.L. Penn, Phase transformation and particle-mediated growth in the formation of hematite from 2-line ferrihydrite, Cryst. Growth Des. 16 (2016) 922–932.
[77] C. Frandsen, B.A. Legg, L.R. Comolli, H. Zhang, B. Gilbert, E. Johnson, J. F. Banfield, Aggregation-induced growth and transformation of β-FeOOH nanorods to micron-sized α-Fe_2O_3 spindles, CrystEngComm 16 (2014) 1451–1458.
[78] J. Baumgartner, A. Dey, P.H. Bomans, C. Le Coadou, P. Fratzl, N.A. Sommerdijk, D. Faivre, Nucleation and growth of magnetite from solution, Nat. Mater. 12 (2013) 310–314.
[79] M. Collepardi, S. Monosi, G. Moriconi, M. Corradi, Tetracalcium aluminoferrite hydration in the presence of lime and gypsum, Cem. Concr. Res. 9 (1979) 431–437.

[80] M. Fukuhara, S. Goto, K. Asaga, M. Daimon, R. Kondo, Mechanisms and kinetics of C4AF hydration with gypsum, Cem. Concr. Res. 11 (1981) 407–414.
[81] G. Möschner, B. Lothenbach, R. Figi, R. Kretzschmar, Influence of citric acid on the hydration of Portland cement, Cem. Concr. Res. 39 (2009) 275–282.
[82] A.C. Cismasu, F.M. Michel, A.P. Tcaciuc, G.E. Brown Jr., Properties of impurity-bearing ferrihydrite III. Effects of Si on the structure of 2-line ferrihydrite, Geochim. Cosmochim. Acta 133 (2014) 168–185.
[83] G. Waychunas, C. Fuller, B. Rea, J. Davis, Wide angle X-ray scattering (WAXS) study of "two-line" ferrihydrite structure: effect of arsenate sorption and counterion variation and comparison with EXAFS results, Geochim. Cosmochim. Acta 60 (1996) 1765–1781.
[84] P.-J. Thibault, D.G. Rancourt, R.J. Evans, J.E. Dutrizac, Mineralogical confirmation of a near-P:Fe = 1:2 limiting stoichiometric ratio in colloidal P-bearing ferrihydrite-like hydrous ferric oxide, Geochim. Cosmochim. Acta 73 (2009) 364–376.
[85] J. Bourdoiseau, R. Sabot, M. Jeannin, F. Termemil, P. Refait, Determination of standard Gibbs free energy of formation of green rusts and its application to the Fe (II–III) hydroxy-oxalate, Colloids Surf. A Physicochem. Eng. Asp. 410 (2012) 72–80.
[86] C. Van Genuchten, T. Behrends, P. Kraal, S.L. Stipp, K. Dideriksen, Controls on the formation of Fe (II, III)(hydr)oxides by Fe(0) electrolysis, Electrochim. Acta 286 (2018) 324–338.
[87] M. Stefanoni, Z. Zhang, U.M. Angst, B. Elsener, The kinetic competition between transport and oxidation of ferrous ions governs precipitation of corrosion products in carbonated concrete, RILEM Techn. Lett. 3 (2018) 8–16.
[88] W. Ostwald, Studien über die Bildung und Umwandlung fester Körper, Z. Phys. Chem. 22 (1897) 289–330.
[89] M. Wolthers, G. Nehrke, J.P. Gustafsson, P. Van Cappellen, Calcite growth kinetics: modeling the effect of solution stoichiometry, Geochim. Cosmochim. Acta 77 (2012) 121–134.
[90] F.J. Millero, S. Sotolongo, M. Izaguirre, The oxidation kinetics of Fe(II) in seawater, Geochim. Cosmochim. Acta 51 (1987) 793–801.